ENCIT 2018

ABCM Associação Brasileira de Engenharia e Ciências Mecânicas

17th Brazilian Congress of Thermal Sciences and Engineering
November 25th-28th, 2018, Águas de Lindóia, SP, Brazil

ENCIT-2018-0468
UNSTABLE TRANSVERSE ROLLS INDUCED BY VISCOUS DISSIPATION FOR A THIN FILM FLOW

Eduardo V. M. dos Reis
L.S. de B. Alves
Departamento de Engenharia Mecânica, Universidade Federal Fluminense, Rua Passo da Pátria 156, Niterói, RJ 24210-240, Brasil
eduardovillela@id.uff.br

Abstract. *Unstable transverse rolls of a thin liquid film is carried out in this paper. The instability is triggered by surface tension gradients, instead of buoyancy effect. This mechanism is known as the Marangoni effect. The only inner heat source is viscous dissipation. The film lower boundary is considered adiabatic and the upper film surface is subjected to convection. In order to investigate the instability of the physical system, the normal mode technique was employed. The steady flow can be determined analytically, but the unstable transverse rolls required numerical procedures to be solved. For this, Runge-Kutta and shooting method were combined to solve the system of equations derived.*

Keywords: *Marangoni effect, Linear Stability Analysis, Viscous dissipation*

1. INTRODUCTION

Instability caused by buoyancy is well known as Rayleigh-Bénard convection (Bénard (1901)). Rayleigh credited this phenomenon to buoyancy effect, which is causes by density gradients (Rayleigh (1916)). Nevertheless, later studies proved that the phenomenon observed by Bénard was driven by another mechanism. Block (1956) showed that convective cells in a thin fluid flow (less than 1mm), such as the one observed by Bénard, could not happen due to buoyancy. Rather this instability must be triggered by another phenomenon: surface tension, known as the Marangoni effect. Soon afterwards, Pearson (1958) showed an analytical explanation for the problem. As a matter of fact, both mechanisms have been studied simultaneously in order to catch the onset of instability (Reichenbach and Linde (1981),Nield (1964)). These studies led to the conclusion that both agencies causing instability reinforce one another and are tightly coupled. However, under microgravity and microscale fluid systems, buoyancy effect becomes negligible, and the Marangoni effect alone is responsible for convection. Some examples of applications of thin film fluids can be found in Craster and Matar (2009).

The Marangoni effect is responsible for being the main mechanism to drive flow motion. Many applications can be found at Scriven and Sternling (1960). In the context of engineering, for example, the Marangoni effect plays a crucial role in the physics of welding. Among other forces acting on a drop at the electrode tip in gas metal arc welding (GMAW), for example, such as the electromagnetic and gravity forces, surface tension plays an import role in transferring metal from the electrode tip to the welding pool. The type of metal transfer has a direct influence on the quality of a welding (Lancaster (1984)).

In order to determine the onset of instability of any dynamical system, the well-established method known as Linear Stability Analysis (LSA) is used. This methodology provides the response of a dynamical system when its steady state is subjected to small disturbances. In order to do so, the original nonlinear governing equations are transformed into linear via Taylor expansion around the steady state. The perturbation is considered modal. Although this method is employed mainly in the context of fluid mechanics problems, some studies involving fluid structure have been carried out as well (dos Reis *et al.*, 2018);Dowell and Hall (2001)). In such context, normal mode shapes and natural frequencies of a structure can be determined, as well as the onset of structural instabilities, such as buckling.

Back to the field of fluid mechanics, it can be found in the literature some examples of flows analysed via LSA, such as Couette-Rayleigh-Bernard(Barletta and Nield (2012)) and Poiseuille-Rayleigh-Bernard(Barletta *et al.* (2011)) convection. Both take into consideration viscous dissipation. Nevertheless, the effect of viscous dissipation as the only source of inner heat generation has only been carried out by Celli *et al.* (2015). This paper offers an extension of the study initiated by Celli *et al.* (2015), but now considering a wider range of parameters, which means the study developed here covers a wider variety of fluids.

In the forthcoming sections, we discuss the stability of a thin film of a Newtonian fluid flowing over an adiabatic plate with a nondeformable surface, and subjected to convection at the free boundary. The onset of instability begins at the

free surface due to surface tension gradients alone, since buoyancy can be neglected from the analyses. It is worthwhile mentioning the Reynolds number must be kept small enough in order to the thermoconvective instability to be the first mechanism that drives convection within the fluid.

2. MATHEMATICAL MODEL

This problem studies a Newtonian film flowing over a plate. This plate is considered adiabatic and impermeable. The upper film surface is a free nondeformable surface and subjected to surface tension and convection as well. Viscous dissipation is the only source of heat generation. The density of the fluid is considered constant since buoyancy effects are neglected. This assumption becomes valid either under micro gravity environments or with thin films. Fig.1 shows a sketch of the physical problem and its steady state

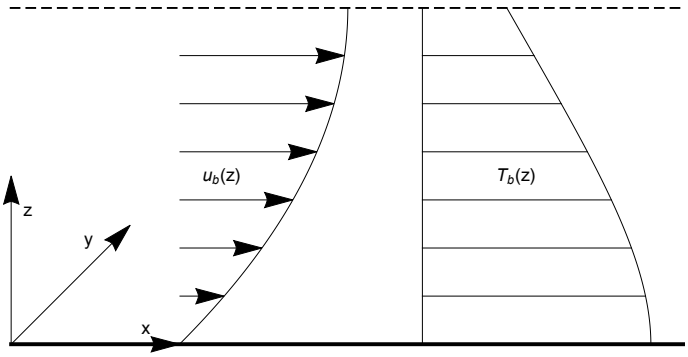

Figure 1. Sketch of the physical problem and the steady flow velocity and temperature profiles, respectively.

The problem governing equations are the local mass conservation, linear momentum and energy balance

$$\nabla.\mathbf{u} = 0 \qquad \frac{\partial \mathbf{u}}{\partial t} + \mathbf{u}.\nabla.\mathbf{u} = -\frac{\nabla P}{\rho} + \nu.\nabla^2\mathbf{u} \qquad \frac{\partial T}{\partial t} + \mathbf{u}.\nabla T = \alpha\nabla^2 T + \frac{2\nu}{c} D_{ij}D_{ij} \tag{1}$$

where **u**=(u, v, w) is the velocity vector, t is time, P is the dynamical pressure, ρ is the specific mass, ν is the kinematic viscosity, T is the temperature, α is the heat diffusivity, c is the specific heat and D is the strain tensor, where repeated index yields summation

$$D_{ij} = \frac{1}{2}\left(\frac{\partial u_i}{\partial x_j} + \frac{\partial u_j}{\partial x_i}\right) \tag{2}$$

where **x**=(x, y, z) is the cartesian position vector. The following step is to model the surface tension as a function of temperature gradients. As pointed out by Selby (1890), for small ranges of temperature, surface tension can be considered linear. As in the theory of LSA the perturbation is considered small enough for the linearized problem to be valid, a liner model is thus used, namely $S = S_0 - \sigma(T - T_0)$, where S is the surface tension and σ is a constant, defined as a surface tension variation with temperature $\partial S/\partial T$.

At this point, we are ready to formulate the boundary conditions. Since the lower film lies on an impermeable plate and its upper free surface is nondeformable and subjected to surface tension and convection, the system of boundary conditions becomes

$$\begin{aligned} &\underline{for \quad z = 0} \\ &u = v = w = 0, \quad \frac{\partial T}{\partial z} = 0 \\ &\underline{for \quad z = 1} \\ &\frac{\partial u}{\partial z} = -\frac{\sigma}{\mu}\frac{\partial T}{\partial x}, \quad \frac{\partial v}{\partial z} = -\frac{\sigma}{\mu}\frac{\partial T}{\partial y}, \quad w = 0, \quad \frac{\partial T}{\partial z} + \frac{h}{k}(T - T_\infty) = 0 \end{aligned} \tag{3}$$

where μ is the dynamic viscosity, h is the external heat transfer coefficient, k is the thermal conductivity, T_∞ is the temperature outside the fluid film at a very large distance form the film surface. Fig.1 displays the physical problem and the boundary conditions used.

In order to reduce the number of parameters, Eq.1 must be written into its dimensionless form. The scaling used is

$$\frac{\alpha}{H^2}t \to t, \frac{\mathbf{x}}{H} \to \mathbf{x}, \frac{H}{\alpha}\mathbf{u} \to \mathbf{u}, \frac{T - T_\infty}{\Delta T} \to T, \frac{H^2}{\mu\alpha}P \to P, \frac{H^2}{\alpha}D_{ij} \to D_{ij}, H\nabla \to \nabla \tag{4}$$

After substituting Eq.4 into Eq.1, one obtains its dimensionless form, which yields

$$\nabla.\mathbf{u} = 0, \qquad \frac{\partial \mathbf{u}}{\partial t} + \mathbf{u}.\nabla.\mathbf{u} = Pr\left(-\nabla P + \nabla^2\mathbf{u}\right), \qquad \frac{\partial T}{\partial t} + \mathbf{u}.\nabla T = \nabla^2 T + 2D_{ij}D_{ij} \tag{5}$$

with the following boundary conditions

$$\begin{aligned} &\underline{for \quad z = 0} \\ &u = v = w = 0, \quad \frac{\partial T}{\partial z} = 0 \\ &\underline{for \quad z = 1} \\ &\frac{\partial u}{\partial z} = -Ma\frac{\partial T}{\partial x}, \quad \frac{\partial v}{\partial z} = -Ma\frac{\partial T}{\partial y}, \quad w = 0, \quad \frac{\partial T}{\partial z} + Bi.T = 0 \end{aligned} \tag{6}$$

Ultimately, the governing parameters that arise after this scaling are

$$Bi = \frac{Hh}{k}, \quad Pr = \frac{\nu}{\alpha}, \quad Ma = \frac{\sigma H \Delta T}{\alpha\mu} \tag{7}$$

with $\Delta T = \nu\alpha/H^2 c$, and where Bi is the Biot number, which represents the ratio between heat flow through convection at the interface and conduction within the fluid; Pr is the Prandtl number, which represents the ratio between linear momentum and energy diffusion; and, finally, Ma is the Marangoni number, which yields the ratio between the sensibility of surface tension with variation of temperature (given by σ) and the sensibility of temperature with variation of energy dissipated (heat capacity). In order to the flow to reach instability threshold, the higher the values of Ma the sooner the flow becomes unstable.

2.1 STEADY STATE

The steady flow is considered fully developed, hence being invariant in the flow direction. It is worthwhile mentioning that the pressure term ∇P in Eq.1 is a dynamic pressure gradient, i.e., it includes the effect of either static pressure and gravity body force. Therefore, the steady flow can be induced either by static pressure gradient or gravitational force alone (if the flow direction is inclined with respect to the vertical direction). In both cases the steady flow profile is the same.

In a fully developed flow, temperature and velocity fields depend only on the nonhomogeneous direction, i.e., the z coordinate, according to Fig.1. Solving Eq.1, one obtains the steady flow solution

$$P_b(x) = Ax + B. \qquad \mathbf{u}_b(z) = \frac{Az}{2}(z-2)\mathbf{n} \qquad T_b(z) = \frac{A^2}{12}\left(3 - 6z^2 + 4z^3 - z^4 + \frac{4}{Bi}\right) \tag{8}$$

where $\mathbf{n}= (1, 0, 0)$, A and B are constants, and the subscript b denotes the basic (steady) state. The constant A can be determined invoking the Péclet number Pe, and assuming Pe to be equal to the average value of the basic flow velocity over the film section.

$$Pe = \int_0^1 \mathbf{u}_b\mathbf{n}dz \longrightarrow A = -3Pe \tag{9}$$

2.2 LINEAR STABILITY ANALYSIS

In order to perform the linear stability analysis, it is necessary to assume the velocity vector, pressure and temperature fields to be composed of steady state profile and a small perturbation of any kind, namely

$$\begin{aligned} \mathbf{u} &= \mathbf{u}_b(z) + \epsilon\mathbf{U}_p(z)e^{i(\alpha x + \beta y - \omega t)} \\ P &= P_b(x) + \epsilon\psi_p(z)e^{i(\alpha x + \beta y - \omega t)} \\ T &= T_b(z) + \epsilon\Theta_p(z)e^{i(\alpha x + \beta y - \omega t)} \end{aligned} \tag{10}$$

where ϵ is a constant assumed small enough to neglect the contributions of higher order terms, i is the complex number $\sqrt{-1}$, α and β are wave numbers in the x and y directions, respectively, and ω is the angular frequency. As one might notice, the perturbation is nonhomogeneous in the z direction, and hence subjected to the boundary conditions. In the x and y directions, on the other hand, the perturbation has a modal behaviour.

In the next step, one must substitute Eq.10 into the dimensionless governing equation, namely Eq.5, obtaining

$$
\begin{aligned}
&i(\alpha u_p + \beta v_p) + {w_p}' = 0, && \text{(11a)}\\
&(Pr(\alpha^2+\beta^2) - i\omega + i\alpha u_b)u_p + iPr\alpha\psi_p + w_p{u_b}' - Pr{u_p}'' = 0, && \text{(11b)}\\
&(Pr(\alpha^2+\beta^2) - i\omega + i\alpha u_b)v_p + iPr\beta\psi_p - Pr{v_p}'' = 0, && \text{(11c)}\\
&(Pr(\alpha^2+\beta^2) - i\omega + i\alpha u_b)w_p(z) + Pr({\psi_p}' - {w_p}'') = 0, && \text{(11d)}\\
&(\alpha^2+\beta^2 - i\omega + i\alpha u_b)\Theta_p + w_p({T_b}' + -2i\alpha {u_b}') - 2{u_b}'{u_p}' - {\Theta_p}'' = 0 && \text{(11e)}
\end{aligned}
$$

The system given by Eq.11 above cannot be solved a priori because the boundary conditions of pressure is unknown. One can overcome this problem by invoking Orr-Sommerfeld equation. Moreover, i) Eq.11b and Eq.11c were combined into a new equation and ii) the second derivative of Eq.11a was obtained, since the continuity equation (Eq.11a) and its first derivative were used to obtain two new boundary conditions for w_p. Finally, one obtains the system of equations (Eq.12) which can be solved numerically and the new boundary conditions derived (Eq.13).

$$
\begin{aligned}
&i(\alpha {u_p}'' + \beta {v_p}'') + {w_p}''' = 0,\\
&\alpha(Pr(\alpha^2+\beta^2) - i\omega + i\alpha u_b) - \beta(Pr(\alpha^2+\beta^2) - i\omega + i\alpha u_b) - \beta w_p u_b' + Pr(\beta u_p'' - \alpha v_p'') = 0\\
&(-(\alpha^2+\beta^2)(Pr(\alpha^2+\beta^2) - i\omega + i\alpha u_b)w_p - i\alpha u_b'') + (2Pr(\alpha^2+\beta^2) - i\omega + i\alpha u_b(z))w_p'' - Prw_p^{(iv)} = 0\\
&(\alpha^2+\beta^2 - i\omega + i\alpha u_b)\Theta_p + w_p({T_b}'(z) + -2i\alpha {u_b}') - 2{u_b}'{u_p}' - {\Theta_p}'' = 0
\end{aligned}
\tag{12}
$$

$$
\begin{aligned}
&\underline{for \quad z = 0}\\
&u_p = v_p = w_p = w_p' = 0, \quad \Theta_p' = 0\\
&\underline{for \quad z = 1}\\
&{u_p}' = -i\alpha Ma\Theta_p,\\
&{v_p}' = -i\beta Ma\Theta_p,\\
&w_p = 0,\\
&w_p'' = -Ma(\alpha^2+\beta^2)\Theta_p,\\
&{\Theta_p}' + Bi\Theta_p = 0
\end{aligned}
\tag{13}
$$

This system of Eq.12 was solved numerically using a Runge-Kutta algorithm coupled with the shooting-method. Both these procedures were implemented in the software *Mathematica 10* using the built-in functions *NDSolve* and *FindRoot*.

3. RESULTS: TRANSVERSE ROLLS

Transverse rolls are defined by perturbations which are invariant in the y direction. Physically, wavelike disturbances travel parallel to the base flow direction.

As the transverse rolls are invariant in the y direction, we set $\beta = 0$ in Eq.12. Therefore, the system of eigenvalue ODE and its boundary conditions become

$$
\begin{aligned}
&i\alpha {u_p}'' + {w_p}''' = 0,\\
&(Pr\alpha^2 - i\omega + i\alpha u_b)\alpha v_p - Pr\alpha v_p'' = 0\\
&(-\alpha^2(Pr\alpha^2 - i\omega + i\alpha u_b) - i\alpha u_b'')w_p + (2Pr\alpha^2 - i\omega + i\alpha u_b(z))w_p'' - Prw_p^{(iv)} = 0\\
&(\alpha^2 - i\omega + i\alpha u_b)\Theta_p + w_p({T_b}'(z) + -2i\alpha {u_b}') - 2{u_b}'{u_p}' - {\Theta_p}'' = 0
\end{aligned}
\tag{14}
$$

$$
\begin{aligned}
&\underline{for \quad z=0} \\
&u_p = v_p = w_p = w_p' = 0, \quad \Theta_p' = 0 \\
&\underline{for \quad z=1} \\
&{u_p}' = -i\alpha Ma\Theta_p, \\
&{v_p}' = 0, \\
&w_p = 0, \\
&w_p'' = -\alpha^2 Ma\Theta_p, \\
&{\Theta_p}' + Bi\Theta_p = 0
\end{aligned}
\tag{15}
$$

3.1 MARGINAL CURVES

Once the system of eigenvalue ODE in Eq.14 with boundary conditions given by Eq.15 is obtained, one now is able to obtain the marginal curve, which stands for the onset of instability. As we performing a temporal analysis, the two eigenvalues are Ma and the angular velocity ω. Fig.2 displays the imminence to instability for different perturbation wavenumber α and for fixed values of the governing parameters, with its corresponding ω displayed in Fig.3.

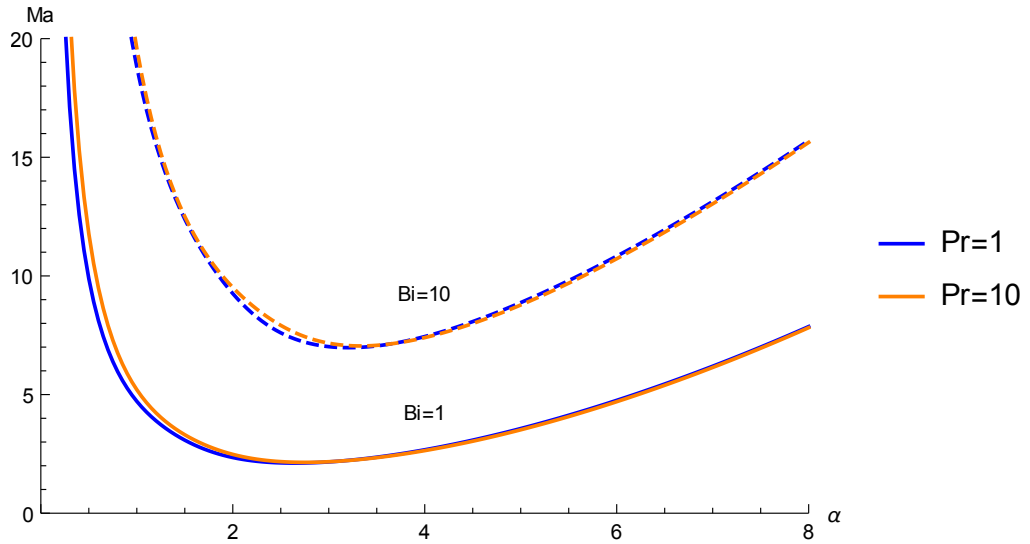

Figure 2. Marginal Curves generated with $Pe = 5$ for $Bi = 1$ (continuous line) and $Bi = 10$ (dashed line), and for $Pr = 1$ (blue line) and $Pr = 10$ (orange line). The eigenvalue Ma indicates the imminence to instability for different pertubation wavenumber.

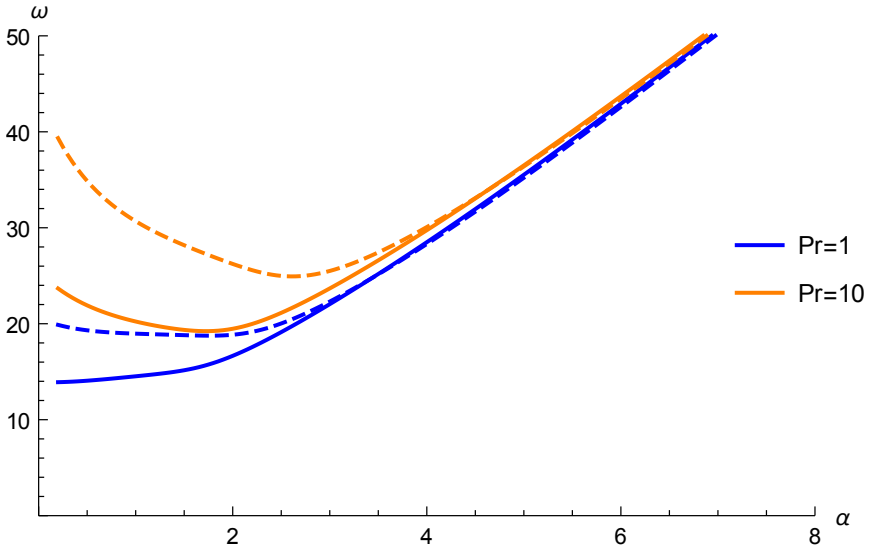

Figure 3. Values of ω generated with $Pe = 5$ for $Bi = 1$ (continuous line) and $Bi = 10$ (dashed line), and for $Pr = 1$ (blue line) and $Pr = 10$ (orange line).

It might be noticed that a change in Pr does not produce significant effect on the marginal curve shape, since the curves for $Pr = 1$ and $Pr = 10$ are almost coincident for the same value of Bi. Later on it will become clear that the value of Pr indeed has little effect on the instability onset, except for $Pr \to 0$.

It is also observed in Fig.2 that the marginal curves seem to jump to infinity as $Bi \to \infty$ for any given value of Pr. In the following section it will be shown that this indeed happens. It turns out that the flow is unconditionally stable when the upper layer is kept isothermal. From a physical point of view it makes sense, since in the limiting case $Bi \to \infty$ any gradient of temperature generated by viscous dissipation is instantaneously sunk by the upper layer convection. Therefore, without temperature gradients the Marangoni effect cannot be allowed to take place and trigger flow instability.

Additionally, the marginal curves in Fig.2 have always an upward concave shape. Disturbances with wavenumbers $\alpha \to 0$ and $\alpha \to \infty$ are stable. There is a specific disturbance wavenumber which triggers first the onset of instability. An analogy can be traced with a mechanical mass spring one degree of freedom oscillator. The system responds at greater amplitudes when the frequency of its forced excitation matches the natural frequency of the system than it does at other frequencies. In other words, frequencies excitation far beyond the natural frequency of the system (below or above) do not generate high amplitude responses (Inman and Singh (1994)). A comparison of this phenomenon can be traced with the marginal curve shape, since there is an optimum perturbation wavenumber which reaches first the onset of instability. Hence, there is always a critical point, which stands for the lowest value of Ma. In the following subsection we discuss the influence of the governing parameters on the critical values of Ma_{cr} and ω_{cr}, as well as the corresponding α_{cr}

As for Fig.3, it displays the angular frequency of perturbation that becomes unstable. The interesting point that can be noticed is that for high values of α the angular frequency tends to assume the same value. Moreover, as the group velocity stands for the slope of the curve, for high values of α the group velocity tends asymptotically to a constant, independently of the value of Pr and Bi. This constant equals to the base flow velocity at the film surface, i.e., $u_b(z = 1, Pe = 5) = 7.5$.

3.2 CRITICAL VALUES

In order to take the critical values Ma_{cr}, ω_{cr} and α_{cr}, the eigenvalues must satisfy the condition $\partial Ma/\partial\alpha = 0$. A method first applied in (Alves *et al.*, 2016) is employed. In this approach, the dispersion relation Eq.12 is derived in function of α, giving rise to another eigenvalue system of ODE. This new system, solved coupled with the dispersion relation given by Eq.12, is able to catch the critical values sought. For the sake of simplicity, this new system derived will not be displayed here.

3.2.1 Influence of Bi

Figures from 4 to 6 show the influence of Bi upon the critical eigenvalues.

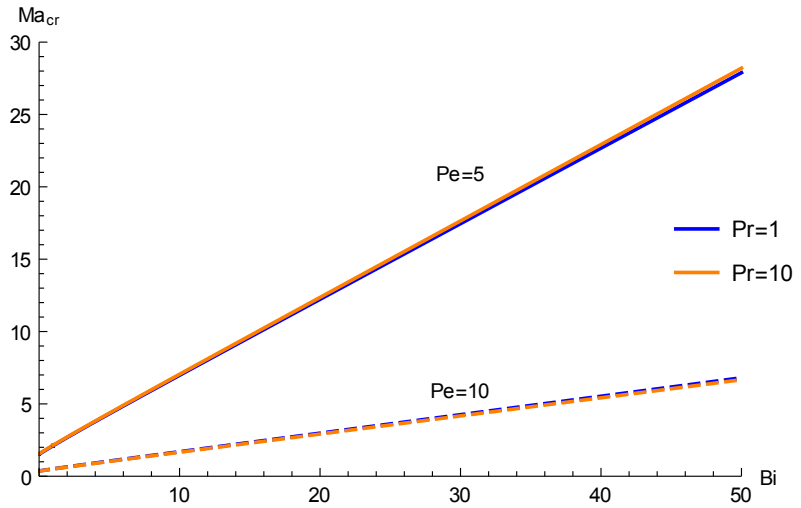

Figure 4. Ma_{cr} as a function of Bi generated for $Pe = 5$ (continuous line) and $Pe = 10$ (dashed line), and for $Pr = 1$ (blue line) and $Pr = 10$ (orange line).

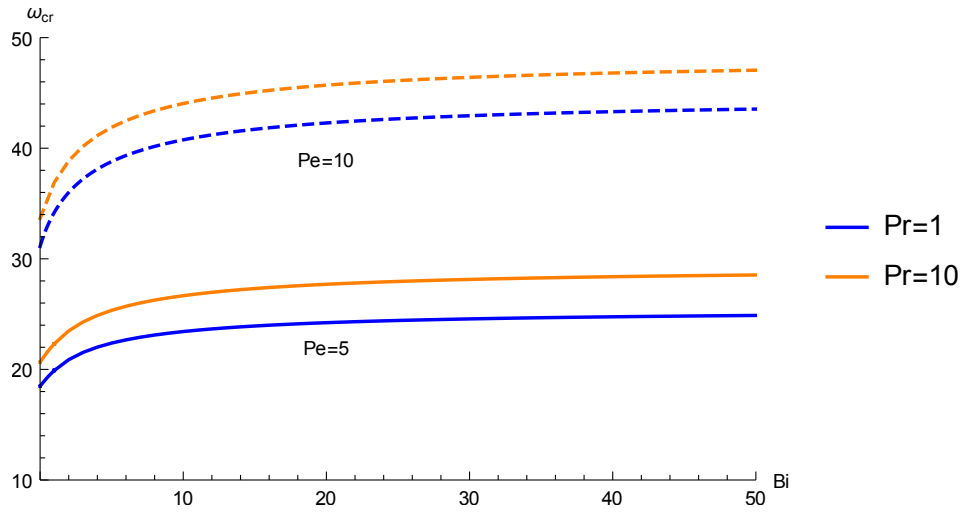

Figure 5. ω_{cr} as a function of Bi generated for $Pe = 5$ (continuous line) and $Pe = 10$ (dashed line), and for $Pr = 1$ (blue line) and $Pr = 10$ (orange line).

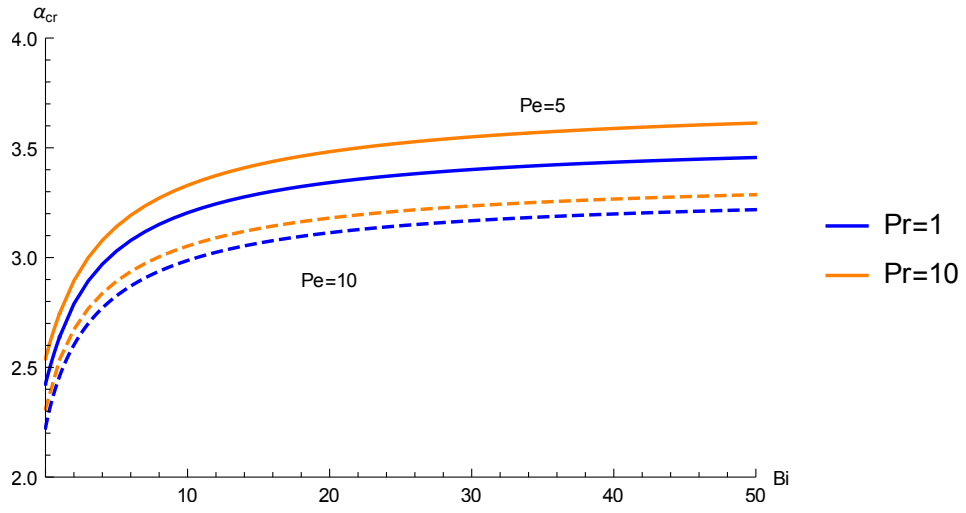

Figure 6. α_{cr} as a function of Bi generated for $Pe = 5$ (continuous line) and $Pe = 10$ (dashed line), and for $Pr = 1$ (blue line) and $Pr = 10$ (orange line).

It can be seen in both Fig.6 and 5 that as $Bi \to 0$, both the critical value α_{cr} and ω_{cr} tend to a constant value. On the other hand, as $Bi \to \infty$, both of them tend asymptotically to another constant value. These values are displayed in Tab.1 and 2 for $Pe = 5$ and $Pe = 10$, respectively.

As for Fig.4, it shows a quasi-linear growth of Ma_{cr} as Bi increases. The first order polynomial approximation for this behaviour is shown in Tab.1 when $Bi \to \infty$. Therefore, it is easy to conclude that under this limiting case the flow is unconditionally stable, as mentioned and physically explained previously.

Table 1. Critical values for the limiting cases $Bi \to 0$ and $Bi \to \infty$ for $Pe = 5$.

	$Bi \to 0$			$Bi \to \infty$		
	α_{cr}	ω_{cr}	Ma_{cr}	α_{cr}	ω_{cr}	Ma_{cr}
$Pr = 1$	2.424	18.475	1.524	3.554	23.435	$1.815 + 0.521Bi$
$Pr = 10$	2.540	20.644	1.557	3.727	29.248	$1.828 + 0.527Bi$

Table 2. Critical values for the limiting cases $Bi \to 0$ and $Bi \to \infty$ for $Pe = 10$.

	$Bi \to 0$			$Bi \to \infty$		
	α_{cr}	ω_{cr}	Ma_{cr}	α_{cr}	ω_{cr}	Ma_{cr}
$Pr = 1$	2.224	31.126	0.364	3.302	44.536	$0.433 + 0.127Bi$
$Pr = 10$	2.312	33.663	0.359	3.379	48.189	$0.421 + 0.125Bi$

3.2.2 Influence of Pr

Below one can find the influence of Pr on the critical eigenvalues

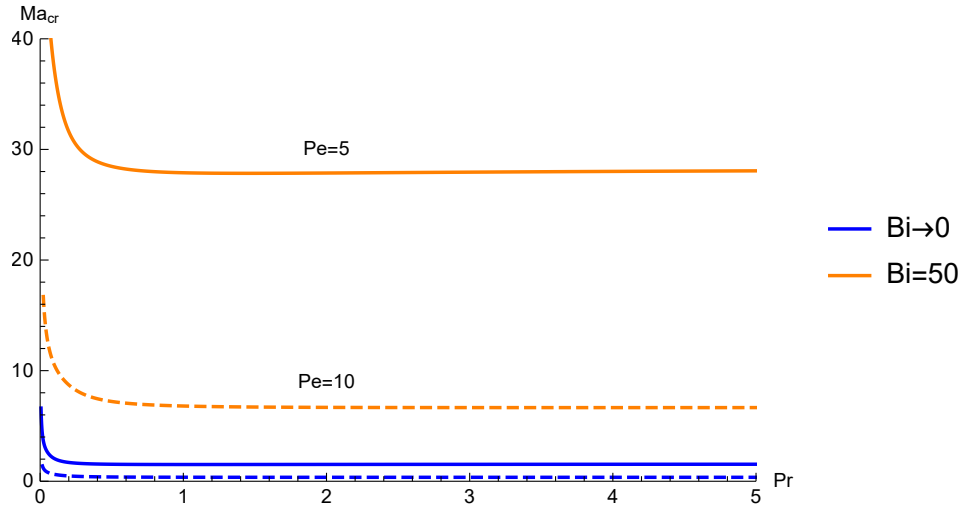

Figure 7. Ma_{cr} as a function of Pr generated for $Pe = 5$ (continuous line) and $Pe = 10$ (dashed line), and for $Bi \to 0$ (blue line) and $Bi = 50$ (orange line).

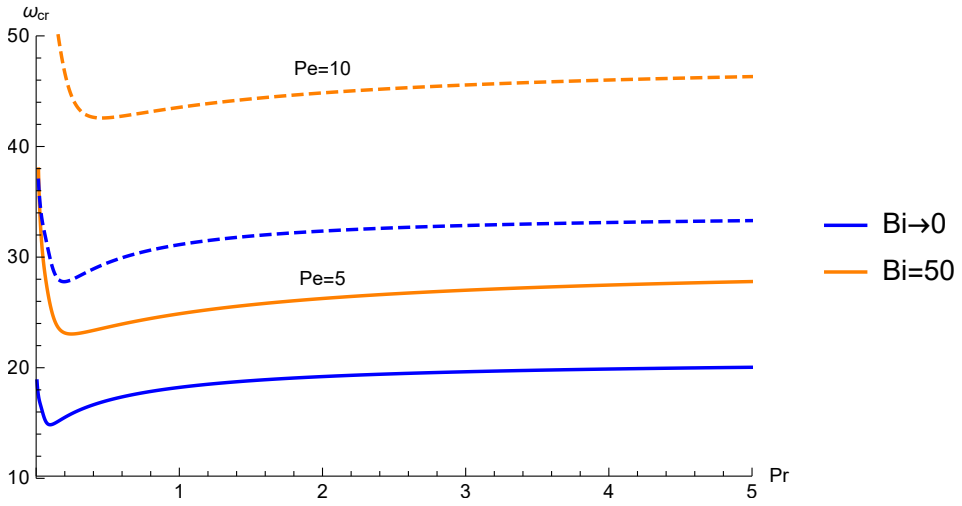

Figure 8. ω_{cr} as a function of Pr generated for $Pe = 5$ (continuous line) and $Pe = 10$ (dashed line), and for $Bi \to 0$ (blue line) and $Bi = 50$ (orange line).

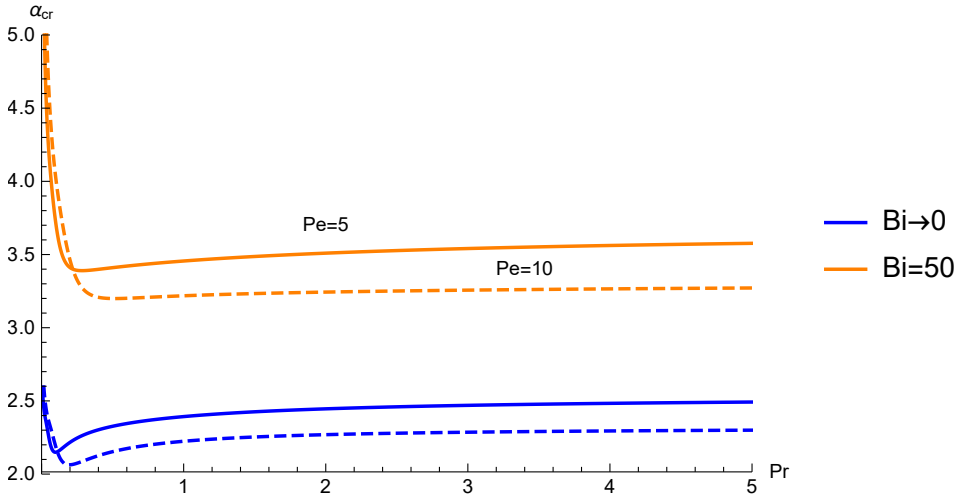

Figure 9. α_{cr} as a function of Pr generated for $Pe = 5$ (continuous line) and $Pe = 10$ (dashed line), and for $Bi \to 0$ (blue line) and $Bi = 50$ (orange line).

Likewise Fig.6 and 5, in both limiting cases $Pr \to 0$ and $Pr \to \infty$ the critical wavenumber α_{cr} and angular frequency ω_{cr} are finite constant values, as shown in Fig.8 and 9. These values are displayed in Tab.3 and 4.

In Fig.7 one can notice that in the limiting case $Pr \to 0$ the problem becomes stable, as $Ma_{cr} \to \infty$. This conclusion is already expected, since when $Pr \to 0$ either $\nu \to 0$ or the heat capacity $\alpha \to \infty$. In the first case, it means no inner heat is allowed to be generated. Therefore, no temperature gradients can take place at the interface of the film, and thus the thermoconvective instability can not be triggered. In the second case, as the heat capacity $\alpha \to \infty$, any perturbation of the temperature gradient field will be instantaneously dissipated, which means no gradients of surface tension is allowed as well, and therefore the flow is unconditionally stable. It is the same phenomenon that happens when $Bi \to \infty$, as already mentioned, but for a different physical mechanisms. Although such low values for Pr are not commonly encountered in general applications, there are a few exceptions like liquid metal, which can reach values of $O(10^{-3})$ (Mills, 1999).

Moreover, analysing the other limit of Pr, Fig.7 shows that Ma_{cr} tends asymptotically to a constant value as $Pr \to \infty$. And it tends very quickly, since when $Pr = 10$, for example, Ma_{cr} reached $\sim 99\%$ of the asymptotic value displayed in Tab. 3 and 4. Physically speaking, the limit case $Pr \to \infty$ implies viscosity going to infinity. Viscosity has two opposite influences on the stability: i) it tends to stabilize the flow, since it accounts for dissipation of linear momentum; and ii) it accounts for generating more intense gradients of temperature, and thus increasing the Marangoni effect. When Pr is high enough, both effects tend to equilibrate each other, and then any further increase in Pr does not affect the flow stability any longer.

Table 3. Critical values for the limiting cases $Bi \to 0$ and $Bi \to \infty$ for $Pe = 5$.

	$Bi \to 0$			$Bi \to \infty$		
	α_{cr}	ω_{cr}	Ma_{cr}	α_{cr}	ω_{cr}	Ma_{cr}
$Bi \to 0$	2.819	20.831	∞	2.532	20.726	1.560
$Bi = 50$	7.426	54.992	∞	3.659	29.441	28.384

Table 4. Critical values for the limiting cases $Bi \to 0$ and $Bi \to \infty$ for $Pe = 10$.

	$Bi \to 0$			$Bi \to \infty$		
	α_{cr}	ω_{cr}	Ma_{cr}	α_{cr}	ω_{cr}	Ma_{cr}
$Bi \to 0$	3.013	44.229	∞	2.322	34.051	0.360
$Bi = 50$	8.285	122.789	∞	3.307	47.967	6.694

3.2.3 Influence of Pe

The influence of Pe on the critical eigenvalues are displayed in Fig.12, 11 and 10.

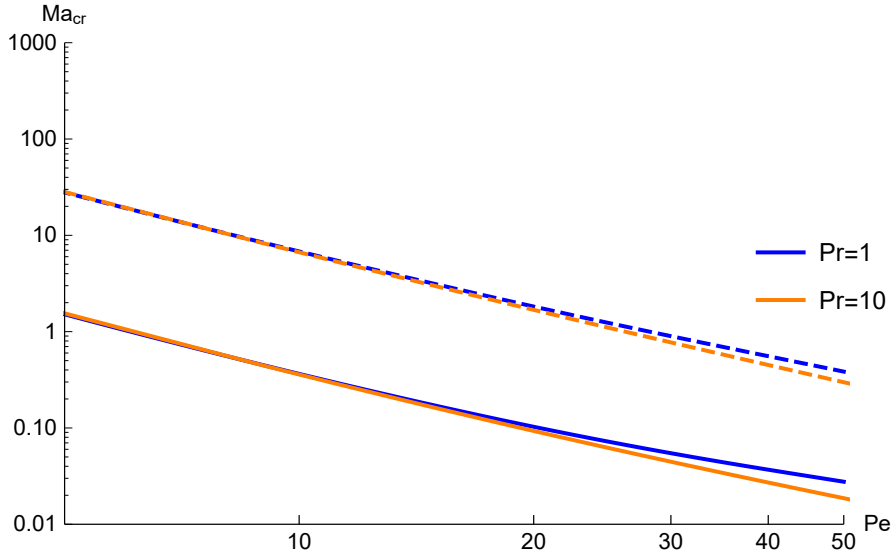

Figure 10. Ma_{cr} as a function of Pr generated for $Pe = 5$ (continuous line) and $Pe = 10$ (dashed line), and for $Bi \to 0$ (blue line) and $Bi = 50$ (orange line).

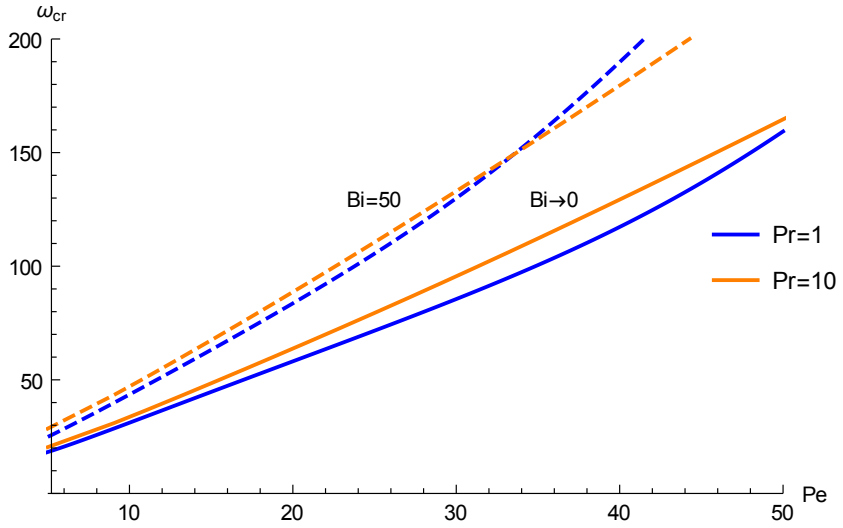

Figure 11. ω_{cr} as a function of Pr generated for $Pe = 5$ (continuous line) and $Pe = 10$ (dashed line), and for $Bi \to 0$ (blue line) and $Bi = 50$ (orange line).

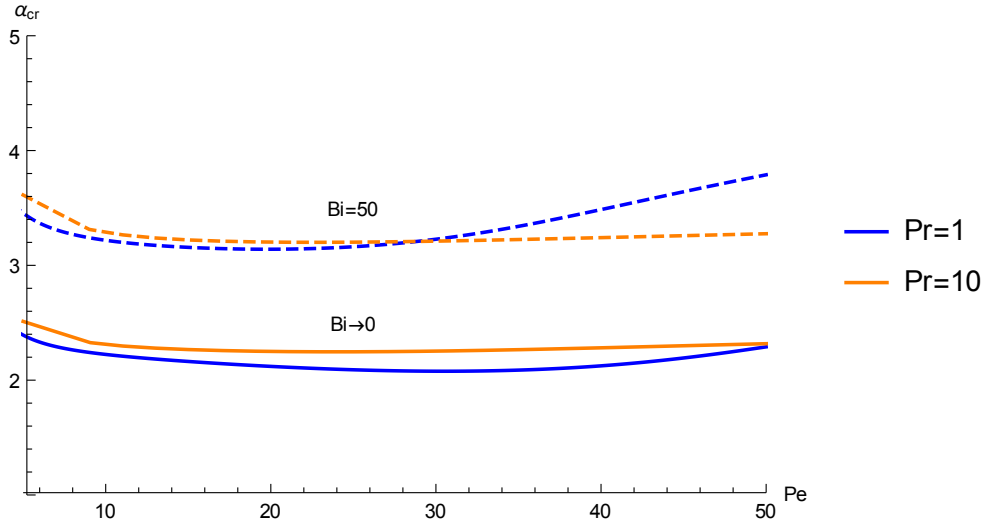

Figure 12. α_{cr} as a function of Pr generated for $Pe = 5$ (continuous line) and $Pe = 10$ (dashed line), and for $Bi \to 0$ (blue line) and $Bi = 50$ (orange line).

As expected, Ma_{cr} tends asymptotically to zero as Pe increases. It is worthwhile recalling that we study the stability triggered by surface tension effect, and not hydrodynamics effects. Therefore, the destabilizing effect of Pe in the flow does not happen due to the inertial forces becoming greater than the viscous forces up to a point where the flow cannot withstand laminar profile any longer under the influence of small disturbances. Rather the influence of Pe takes place due its effect on the steady flow. Higher values of Pe stands for higher gradients of velocity and temperature of the steady profile. The more intense (higher gradients) the steady is, the less stable it becomes.

In Fig.11 and 12 one can see that the value of ω_{cr} and α_{cr} keeps increasing as Pe increases, independently of the value of Bi.

4. CONCLUSIONS

The instability of a thin liquid film flowing over a horizontal adiabatic plate was analysed. Only the transverse rolls were carried out in this paper. The upper surface is subjected to Robin boundary condition (convection). The instability trigger takes place due to surface tension gradients, known as Marangoni effect. The normal mode method was used to perform the linear stability analysis. A simple linear model was used to model surface tension as a function of temperature. After writing the governing equations into its dimensionless form, a system of four differential equation for the perturbation motion was obtained and four governing parameters arisen, namely Bi, which stands for convection through the upper liquid film, Pe, which stands for the flow intensity and temperature steady profile, and, finally, Pr, which is a

parameter that depends only on the fluids properties, and stands for the relation between viscous and heat diffusion. This system was solved numerically by means of the software *Mathematica 10*. The main conclusions can be summarized as follows

i) The marginal curves defining the onset of instability were plotted. It was shown that for disturbances $\alpha \to 0$ and $\alpha \to \infty$ the problem is stable.

ii)There is a critical value of wavenumber disturbance that triggers first the instability. The associated eigenvalues Ma_{cr}, ω_{cr} and α_{cr} were plotted in function of the governing parameters Bi, Pr and Pe.

iii) Increasing values of Bi moves the marginal curves upward, hence stabilizing the problem. As $Bi \to \infty$, the relation of Ma_{cr} with Bi can be written in terms of a linear polynomial. As for the relation of α_{cr} and ω_{cr}, they tend monotonically to a specific value.

iv) The marginal curve does not change significantly as a function of Pr. In fact, for $Pr \geq 10$ the relative difference between Ma_{cr} and its value evaluated with $Pr \to \infty$ stays within 1%.

v) The value of Pr only plays a crucial influence on the instability threshold when Pr is not small enough. Under the limit condition $Pr \to 0$, the flow is unconditionally stable, since no heat generation is allowed. On the other limit extreme, as $Pr \to$, both the effects of destabilizing (viscous heat generation) and stabilizing (linear moment diffusion) reach equilibrium, and therefore the value of Pr does not take part in the threshold stability. It is interesting that this equilibrium is reached for still low values of Pr, namely $Pr \geq\sim 10$.

vi) Pe has a destabilizing impact on the flow due to its contribution to increase the gradients of velocity and temperature of the steady profile.

5. ACKNOWLEDGEMENTS

The authors would like to acknowledge CNPq and CAPES for the financial support.

6. REFERENCES

Alves, L.S.d.B., Hirata, S.C. and Ouarzazi, M.N., 2016. "Linear onset of convective instability for rayleigh-bénard-couette flows of viscoelastic fluids". *Journal of Non-Newtonian Fluid Mechanics*, Vol. 231, pp. 79–90.

Barletta, A., Celli, M. and Nield, D., 2011. "On the onset of dissipation thermal instability for the poiseuille flow of a highly viscous fluid in a horizontal channel". *Journal of Fluid Mechanics*, Vol. 681, pp. 499–514.

Barletta, A. and Nield, D., 2012. "On the rayleigh–bénard–poiseuille problem with internal heat generation". *International Journal of Thermal Sciences*, Vol. 57, pp. 1–16.

Bénard, H., 1901. *Les tourbillons cellulaires dans une nappe liquide propageant de la chaleur par convection: en régime permanent*. Gauthier-Villars.

Block, M.J., 1956. "Surface tension as the cause of bénard cells and surface deformation in a liquid film". *Nature*, Vol. 178, No. 4534, pp. 650–651.

Celli, M., Barletta, A. and Alves, L.S.d.B., 2015. "Marangoni instability of a liquid film flow with viscous dissipation". *Physical Review E*, Vol. 91, No. 2, p. 023006.

Craster, R. and Matar, O., 2009. "Dynamics and stability of thin liquid films". *Reviews of modern physics*, Vol. 81, No. 3, p. 1131.

dos Reis, E., Sphaier, L., Nunes, L. and Alves, L.d.B., 2018. "Dynamic response of free span pipelines via linear and nonlinear stability analyses". *Ocean Engineering*, Vol. 163, pp. 533–543.

Dowell, E.H. and Hall, K.C., 2001. "Modeling of fluid-structure interaction". *Annual review of fluid mechanics*, Vol. 33, No. 1, pp. 445–490.

Inman, D.J. and Singh, R.C., 1994. *Engineering vibration*, Vol. 3. Prentice Hall Englewood Cliffs, NJ.

Lancaster, J., 1984. "Metal transfer and mass flow in the weld pool the physics of welding ed jf lancaster".

Mills, A.F., 1999. *Basic heat and mass transfer*. Pearson College Div.

Nield, D., 1964. "Surface tension and buoyancy effects in cellular convection". *Journal of Fluid Mechanics*, Vol. 19, No. 3, pp. 341–352.

Pearson, J., 1958. "On convection cells induced by surface tension". *Journal of fluid mechanics*, Vol. 4, No. 5, pp. 489–500.

Rayleigh, L., 1916. "Lix. on convection currents in a horizontal layer of fluid, when the higher temperature is on the under side". *The London, Edinburgh, and Dublin Philosophical Magazine and Journal of Science*, Vol. 32, No. 192, pp. 529–546.

Reichenbach, J. and Linde, H., 1981. "Linear perturbation analysis of surface-tension-driven convection at a plane interface (marangoni instability)". *Journal of Colloid and Interface Science*, Vol. 84, No. 2, pp. 433–443.

Scriven, L. and Sternling, C., 1960. "The marangoni effects". *Nature*, Vol. 187, No. 4733, p. 186.

Selby, A., 1890. "On the variation of surface-tension with temperature". *Proceedings of the Physical Society of London*, Vol. 11, No. 1, p. 119.

7. RESPONSIBILITY NOTICE

The authors are the only responsible for the printed material included in this paper.